Valence Tautomerism for Quinone Complexes of Manganese: Members of the $Mn^{IV}(N\text{-}N)(Cat)_2$−$Mn^{III}(N\text{-}N)(SQ)(Cat)$−$Mn^{II}(N\text{-}N)(SQ)_2$ Series

Attia S. Attia† and Cortlandt G. Pierpont*

Department of Chemistry and Biochemistry, University of Colorado, Boulder, Colorado 80309

Received November 30, 1994®

Intramolecular electron transfer has been investigated for members of the Mn(N-N)(3,6-DBQ)$_2$ tautomeric series for complex molecules with both *cis* and *trans* structures prepared with *N*-donor coligands of varying basicity. Characteristic structural features of d^3 Mn(IV), d^4 Mn(III), and d^5 Mn(II) have been used to assign charge distribution for complexes characterized crystallographically. Mn^{IV}(2,2′-bpy)(3,6-DBCat)$_2$ [monoclinic, *C*2/*c*, a = 10.713(2) Å, b = 29.880(4) Å, c = 12.208(2) Å, β = 113.51(1)°, V = 3583(1) Å^3, Z = 4, R = 0.043], *trans*-Mn^{III}(4,4′-bpy)$_2$(3,6-DBSQ)(3,6-DBCat) [monoclinic, $P2_1/n$, a = 14.428(2) Å, b = 10.070(2) Å, c = 19.976(3) Å, β = 109.16(1)°, V = 2741.5(8) Å^3, Z = 2, R = 0.064], and Mn^{II}(NO_2-phen)(3,6-DBSQ)$_2$ [monoclinic, *Pc*, a = 12.753-(3) Å, b = 11.288(3) Å, c = 17.950(4) Å, β = 105.21(2)°, V = 2493(1) Å^3, Z = 2, R = 0.049] are examples of the three tautomers that result from differences in intramolecular Mn−quinone charge distribution. Mn(phen)-(3,6-DBQ)$_2$ [monoclinic, *C*2/*c*, a = 10.502(2) Å, b = 31.151(5) Å, c = 12.324(2) Å, β = 114.02(1)°, V = 3683(1) Å^3, Z = 4, R = 0.052] exists as an equilibrium mixture of Mn(IV) and Mn(III) tautomers in the solid state at room temperature. An intense transition appears characteristically for the Mn(III) tautomers in the 2100 nm region of the infrared. The appearance of a band in this region for Mn(2,2′-bpy)(3,6-DBCat)$_2$ is indicative of a shift to the Mn(III) charge distribution at 350 K in the solid state, and a decrease in the intensity at 2100 nm for Mn(4,4′-bpy)$_2$(3,6-DBSQ)(3,6-DBCat) at 350 K indicates a shift in the Mn(III)/Mn(II) equilibrium toward the Mn(II) tautomer at increased temperature. The Mn(IV) tautomer is favored at low temperature and for hard donor coligands. Shifts in equilibrium to the high-spin $Mn^{II}(SQ)_2$ tautomer at increased temperature are thought to be driven entropically, primarily by the increase in low-frequency vibrational activity that results from the addition of charge to the octahedral e_g σ-antibonding orbital.

Introduction

Transition metal complexes containing semiquinone and catecholate ligands have shown a unique facility for electron transfer between the metal and chelated quinone ligands.[1] This has been most dramatically illustrated for the complexes of cobalt where temperature-dependent equilibria between Co^{III}−Cat and Co^{II}−SQ tautomers have been observed to occur in solution and in the solid state.[2,3]

$$Co^{III}(N\text{-}N)(SQ)(Cat) \rightleftharpoons Co^{II}(N\text{-}N)(SQ)_2 \qquad (1)$$

An intense low-energy transition, near 2500 nm, is characteristically observed for Co(III) forms, and this band has been assigned as the optical Cat → Co(III) CT transition.[2b] The thermal barrier to electron transfer occurs at lower energy, and this is responsible for temperature-dependent shifts in equilibria between the valence tautomers shown in eq 1. Shifts in charge distribution induced either thermally or optically change the chemical reactivity of both the metal and quinone sites and sometimes result in a physical response associated with the change in complex volume.[3a,4,5] On a fundamental level, these complexes offer a unique opportunity for studies on metal−ligand electron transfer under equilibrium conditions.

Shortly after the discovery of tautomeric equilibria for the cobalt complexes, similar observations were made for a related complex of manganese.[6] The Mn(IV) complex Mn(py)$_2$(3,5-DBCat)$_2$ was observed to show a dramatic thermochromic effect in solution. In toluene at temperatures below 240 K, the deep purple color of the complex in the solid state was observed. As solution temperature was increased, the intensity of transitions at 824 and 515 nm that are characteristic of the Mn(IV) tautomer decreased. At the same time, a low-intensity transition at 780 nm appeared, and solution color changed to pale green-brown at room temperature. A similar optical transition had been observed for [Mn^{II}(3,5-DBSQ)$_2$]$_4$, and on this basis, it was concluded that the reversible equilibrium shown in eq 2 involving transfer of two electrons was responsible for the thermochromic effect.

$$Mn^{IV}(py)_2(3,5\text{-}DBCat)_2 \rightleftharpoons Mn^{II}(py)_2(3,5\text{-}DBSQ)_2 \qquad (2)$$

Further studies have been carried out to provide definitive characterization of the Mn(II) component in the tautomeric equilibrium, to observe the Mn(III) intermediate that might be formed in a one-electron transfer step, and to determine whether the shift from the *trans* structure of the complexes containing pyridine ligands to a *cis* structure formed with chelating N-donor coligands influences electron transfer.

† Permanent address: Ain Shams University, Cairo, Egypt.

® Abstract published in *Advance ACS Abstracts,* February 1, 1995.

(1) (a) Pierpont, C. G.; Buchanan, R. M. *Coord. Chem. Rev.* **1981**, *38*, 45. (b) Pierpont, C. G.; Lange, C. W. *Prog. Inorg. Chem.* **1993**, *41*, 381.

(2) (a) Jung, O.-S.; Pierpont, C. G. *J. Am. Chem. Soc.* **1994**, *116*, 1127. (b) Jung, O.-S.; Pierpont, C. G. *Inorg. Chem.* **1994**, *33*, 2227. (c) Buchanan, R. M.; Pierpont, C. G. *J. Am. Chem. Soc.* **1980**, *102*, 4951.

(3) (a) Abakumov, G. A.; Cherkasov, V. K.; Bubnov, M. P.; Ellert, O. G.; Dobrokhotova, Z. B.; Zakharov, L. N.; Struchkov, Y. T. *Dokl. Akad. Nauk SSSR* **1993**, *328*, 12. (b) Adams, D. M.; Dei, A.; Rheingold, A. L.; Hendrickson, D. N. *J. Am. Chem. Soc.* **1993**, *115*, 8221.

(4) Jung, O.-S.; Pierpont, C. G. *J. Am. Chem. Soc.* **1994**, *116*, 2229.

(5) Lange, C. W.; Foldeaki, M.; Nevodchikov, V. I.; Cherkasov, V. K.; Abakumov, G. A.; Pierpont, C. G. *J. Am. Chem. Soc.* **1992**, *114*, 4220.

(6) Lynch, M. W.; Hendrickson, D. N.; Fitzgerald, B. J.; Pierpont, C. G. *J. Am. Chem. Soc.* **1984**, *106*, 2041.

0020-1669/95/1334-1172$09.00/0

Table 1. Crystallographic Data for Mn(2,2′-bpy)(3,6-DBCat)$_2$, Mn(4,4′-bpy)$_2$(3,6-DBSQ)(3,6-DBCat)·2C$_4$H$_8$O$_2$, Mn(NO$_2$-phen)(3,6-DBSQ)$_2$·2C$_7$H$_8$, and Mn(phen)(3,6-DBQ)$_2$[a]

	Mn(2,2′-bpy)(3,6-DBCat)$_2$	Mn(4,4′-bpy)(3,6-DBSQ)(3,6-DBCat)·2C$_4$H$_8$O$_2$	Mn(NO$_2$phen)(3,6-DBSQ)$_2$·2C$_7$H$_8$	Mn(phen)(3,6-DBQ)$_2$
formula	$C_{38}H_{48}N_2O_4Mn$	$C_{56}H_{72}N_4O_8Mn$	$C_{54}H_{63}N_3O_6Mn$	$C_{40}H_{48}N_2O_4Mn$
fw	651.7	984.1	888.9	675.7
color	purple	purple	green-brown	purple
space group	*C*2/*c*	*P*2$_1$/*n*	*Pc*	*C*2/*c*
a (Å)	10.713(2)	14.428(2)	12.753(3)	10.502(2)
b (Å)	29.880(4)	10.070(2)	11.288(3)	31.151(5)
c (Å)	12.208(2)	19.976(3)	17.950(4)	12.324(2)
β (deg)	113.51(1)	109.16(1)	105.21(2)	114.02(1)
v (Å^3)	3583(1)	2741.5(8)	2493(1)	3683(1)
Z	4	2	2	4
T (°C)	24	24	24	24
λ(Mo Kα) (Å)	0.710 73	0.710 73	0.710 73	0.710 73
D_{calcd} (g cm^{-3})	1.208	1.192	1.184	1.219
μ (mm^{-1})	0.391	0.282	0.301	0.382
R, R_w	0.043, 0.053	0.064, 0.065	0.049, 0.056	0.052, 0.058

[a] $R = \sum||F_o| - |F_c||/\sum|F_o|$; $R_w = [\sum w(|F_o| - |F_c|)^2/\sum w(F_o)^2]^{1/2}$.

Experimental Section

Materials. 2,2′-Bipyridine (2,2′-bpy), 4,4′-bipyridine (4,4′-bpy), 1,-10-phenanthroline (phen), and 5-nitro-1,10-phenanthroline (NO$_2$-phen), were purchased from Aldrich. Dimanganese decacarbonyl was purchased from Strem Chemical Co. 3,6-Di-*tert*-butyl-1,2-benzoquinone (3,6-DBBQ) was prepared using a literature procedure.[7]

Complex Syntheses. Mn(2,2′-bpy)(3,6-DBCat). Mn$_2$(CO)$_{10}$ (0.13 g, 0.33 mmol), 3,6-DBBQ (0.29 g, 1.32 mmol), and 2,2′-bipyridine (0.15 g, 1.15 mmol) were dissolved in 50 mL of a degassed thf−hexane (1:4) solution under N$_2$. The solution was irradiated for 20 h with a GE 275-W sun lamp, and the volume of the deep purple solution was reduced with a flow of dry N$_2$. Crystals of Mn(2,2′-bpy)(3,6-DBCat)$_2$ were obtained as dark purple parallelepipeds in greater than 85% yield. The structure of the complex was determined from a crystal obtained directly from the reaction mixture.

Anal. Calc for $C_{38}H_{48}N_2O_4Mn$: C, 70.0; H, 7.4; N, 4.3. Found: C, 69.3; H, 7.8; N, 4.1.

Mn(4,4′-bpy)(3,6-DBSQ)(3,6-DBCat). 3,6-DBBQ (0.35 g, 1.59 mmol) and 4,4′-bipyridine (0.23 g, 1.47 mmol) were dissolved in 50 mL of a degassed thf−ethyl acetate (1:4) solution. The mixture was added to Mn$_2$(CO)$_{10}$ (0.23 g, 1.47 mmol) under N$_2$, and the solution was heated to 70 °C to dissolve the reactants. The solution was then irradiated for 20 h, and during this time purple crystals of Mn(4,4′-bpy)(3,6-DBSQ)(3,6-DBCat) separated from the solution. The product was obtained in 70% yield as the ethyl acetate solvate, Mn(4,4′-bpy)-(3,6-DBSQ)(3,6-DBCat); 2C$_4$H$_8$O$_2$.

Anal. Calc for $C_{56}H_{72}N_4O_8Mn$: C, 68.3; H, 7.4; N, 5.7. Found: C, 65.7; H, 6.8; N, 5.1.

Mn(NO$_2$-phen)(3,6-DBSQ)$_2$. 5-Nitro-1,10-phenanthroline (0.10 g, 0.65 mmol) dissolved in 40 mL of toluene was added to Mn$_2$(CO)$_{10}$ (0.12 g, 0.31 mmol) and 3,6-DBBQ (0.29 g, 1.32 mmol) dissolved in 10 mL of thf under N$_2$. The mixture was irradiated for 8 h, and during this time green-brown crystals of Mn(NO$_2$-phen)(3,6-DBSQ)$_2$ separated from solution. The product was obtained in 57% yield as the toluene solvate, Mn(NO$_2$-phen(3,6-DBSQ)$_2$·2C$_7$H$_8$.

Anal. Calc for $C_{54}H_{63}N_3O_6Mn$: C, 73.0; H, 7.1; N, 4.7. Found: C, 71.3; H, 6.7; N, 4.2.

Mn(phen)(3,6-DBQ)$_2$. Mn$_2$(CO)$_{10}$ (0.15 g, 0.38 mmol), 3,6-DBBQ (0.36 g, 1.64 mmol), and 1,10-phenanthroline (0.12 g, 1.11 mmol) were dissolved in 50 mL of a degassed thf−hexane (1:3) solution under N$_2$. The solution was irradiated for 20 h with a GE 275-W sun lamp, and the volume of the deep purple solution was reduced with a flow of dry N$_2$. Crystals of Mn(phen)(3,6-DBQ)$_2$ were obtained as dark purple parallelepipeds in greater than 85% yield.

Anal. Calc for $C_{40}H_{48}N_2O_4Mn$: C, 71.1; H, 7.2; N, 4.1. Found: C, 70.8; H, 7.4; N, 4.1.

(7) Belostotskaya, I. S.; Komissarova, N. L.; Dzhuaryan, E. V.; Ershov, V. V. *Isv. Akad. Nauk SSSR* **1972**, 1594.

Table 2. Atomic Coordinates (×10^4) and Equivalent Isotropic Displacement Parameters (Å^2, ×10^3) for Selected Atoms of Mn^{IV}(2,2′-bpy)(3,6-DBCat)$_2$

	x/a	*y/b*	*z/c*	*U*(eq)
Mn	5000	669(1)	2500	47(1)
O1	3761(2)	6383(1)	1500(2)	56(1)
O2	5779(2)	6674(1)	1378(2)	50(1)
N1	6291(3)	7244(1)	3158(2)	53(1)
C1	4200(3)	6100(1)	703(2)	44(1)
C2	5334(3)	6317(1)	639(2)	42(1)
C3	5933(3)	6177(1)	−124(2)	44(1)
C4	5310(3)	5808(1)	−831(3)	54(1)
C5	4188(3)	5594(1)	−770(3)	56(1)
C6	3601(3)	5726(1)	1(3)	47(1)
C15	7632(4)	7200(1)	3724(3)	69(2)
C16	8485(5)	7566(2)	3994(3)	94(2)
C17	7926(6)	7982(2)	3667(4)	104(3)
C18	6556(6)	8028(1)	3097(3)	89(2)
C19	5737(3)	7653(1)	2826(2)	60(1)

Physical Measurements. Electronic spectra were recorded on a Perkin-Elmer Lambda 9 spectrophotometer equipped with a RMC-Cryosystems cryostat. Solid samples were prepared as KBr pellets. Magnetic measurements were made using a Quantum Design SQUID magnetometer at a field strength of 5 kG. Infrared spectra were recorded on a Perkin-Elmer 1600 FTIR with samples prepared as KBr pellets.

Crystallographic Structure Determinations. Mn(2,2′-bpy)(3,6-DBCat)$_2$. Dark purple crystals of the complex were obtained directly from the reaction mixture. Axial photographs indicated monoclinic symmetry, and the centered settings of 25 intense reflections with 2θ values between 21 and 34° gave the unit cell dimensions listed in Table 1. Data were collected by $\theta-2\theta$ scans within the angular range 3.0−50°. A Patterson map indicated that the metal atom was located on the 2-fold axis of the space group with $Z = 4$. Phases derived from the location of the Mn gave the positions of other atoms of the structure. Final cycles of refinement converged with discrepancy indices of $R = 0.043$ and $R_w = 0.053$. Selected atomic coordinates are listed in Table 2. Tables containing full listings of atom positions, anisotropic displacement parameters, and hydrogen atom locations are available as supplementary material.

Mn(4,4′-bpy)(3,6-DBSQ)(3,6-DBCat). Dark purple crystals of the complex were obtained directly from the reaction mixture. Axial photographs indicated monoclinic symmetry, and the centered settings of 25 intense reflections with 2θ values between 19 and 32° gave the unit cell dimensions listed in Table 1. Data were collected by $\theta-2\theta$ scans within the angular range 3.0−45°. A Patterson map indicated that the metal atom was located at the origin of the unit cell with $Z = 2$. Phases derived from the location of the Mn gave the positions of other atoms of the molecule. A subsequent difference Fourier map revealed the location of an ethyl acetate solvate molecule at a general

Table 3. Atomic Coordinates ($\times 10^4$) and Equivalent Isotropic Displacement Parameters (Å^2, $\times 10^3$) for Selected Atoms of Mn^{III}(4,4′-bpy)$_2$(3,6-DBSQ)(3,6-DBCat)

	x/a	*y/b*	*z/c*	*U*(eq)
Mn	0	0	0	39(1)
O1	1195(3)	841(4)	61(2)	42(2)
O2	744(3)	−896(4)	830(2)	39(2)
C1	1933(5)	417(6)	619(3)	31(3)
C2	1690(5)	−548(6)	1041(3)	33(3)
C3	2403(5)	−1097(7)	1649(3)	37(3)
C4	3339(5)	−609(7)	1791(3)	41(3)
C5	3580(5)	343(7)	1372(4)	47(3)
C6	2905(5)	889(7)	770(4)	38(3)
N1	−347(4)	1639(7)	664(3)	56(3)
C15	−640(7)	1376(10)	1214(5)	76(5)
C16	−876(7)	2324(11)	1628(5)	82(5)
C17	−826(6)	3651(10)	1493(4)	53(4)
C18	−521(7)	3924(9)	922(5)	79(5)
C19	−297(7)	2923(11)	540(5)	77(5)
N2	−1583(7)	6661(10)	2750(5)	98(5)
C20	−1082(6)	4686(9)	1921(4)	59(4)
C21	−1448(8)	4363(11)	2463(6)	93(6)
C22	−1670(9)	5397(15)	2840(6)	114(7)
C23	−1211(8)	6917(11)	2252(7)	102(6)
C24	−974(7)	6022(12)	1832(6)	87(6)

position in the unit cell. Final cycles of refinement converged with discrepancy indices of $R = 0.064$ and $R_w = 0.065$. Selected atomic coordinates are listed in Table 3. Tables containing full listings of atom positions, anisotropic displacement parameters, and hydrogen atom locations are available as supplementary material.

Mn(NO$_2$-phen)(3,6-DBSQ)$_2$. Green-brown crystals of the complex were grown from a toluene solution. Axial photographs indicated monoclinic symmetry, and the centered settings of 25 intense reflections with 2θ values between 19 and 32° gave the unit cell dimensions listed in Table 1. Data were collected by $\theta-2\theta$ scans within the angular range 3.0−50°. Density measurements together with the unit cell volume indicated that there were two complex molecules per unit cell. The coordinates of the manganese atom were determined using a sharpened Patterson map, and phases generated from the location of this atom gave the positions of other atoms of the structure, including the locations of two toluene solvent molecules of crystallization. Final cycles of refinement converged with discrepancy indices of $R = 0.049$ and $R_w = 0.056$. Selected atomic coordinates are listed in Table 4. Tables containing full listings of atom positions, anisotropic displacement parameters, and hydrogen atom locations are available as supplementary material.

Mn(phen)(3,6-DBQ)$_2$. Dark purple crystals of the complex were obtained directly from the reaction mixture. Axial photographs indicated monoclinic symmetry, and the centered settings of 25 intense reflections with 2θ values between 19 and 36° gave the unit cell dimensions listed in Table 1. Data were collected by $\theta-2\theta$ scans within the angular range 3.0−50°. A Patterson map indicated that the metal atom was located on the 2-fold axis of the space group with $Z = 4$. Phases derived from the location of the Mn gave the positions of other atoms of the structure. Final cycles of refinement converged with discrepancy indices of $R = 0.052$ and $R_w = 0.058$. Selected atomic coordinates are listed in Table 5. Tables containing full listings of atom positions, anisotropic displacement parameters, and hydrogen atom locations are available as supplementary material.

Results

The photolysis of solutions containing $Mn_2(CO)_{10}$ and 3,5-di-*tert*-butyl-1,2-benzoquinone has been used to study benzoquinone oxidative addition to the $Mn(CO)_5$ radical.[8] Stoichiometric reactions lead to the $Mn(CO)_4$(3,5-DBSQ) product by one-electron transfer; reactions carried out with excess 3,5-DBBQ result in formation of the $[Mn^{II}(3,5\text{-DBSQ})_2]_4$ tetramer.[6] Irradiation of solutions containing a mixture of $Mn_2(CO)_{10}$, 3,6-di-*tert*-butyl-1,2-benzoquinone, and nitrogen-donor coligand has been used as a general route to members of the Mn(N-N)(3,6-DBQ)$_2$ series. Coligands used in the present study include 2,2′-bipyridine (2,2′-bpy), 4,4′-bipyridine (4,4′-bpy), 1,10-phenanthroline (phen), and 5-nitro-1,10-phenanthroline (NO$_2$-phen). In research to be described separately, complexes containing pyridine (py), pyrazine (pyz), thf, and 3,6-DBSQ (in Mn^{III}(3,6-DBSQ)$_3$) have been prepared and characterized.[9] Octahedral complexes of d^3 Mn(IV), high-spin d^4 Mn(III), and high-spin d^5 Mn(II) have distinctive structural features that result from population of the $d\sigma$ e_g level. The pattern of bond lengths within the inner coordination sphere has been used to provide information on charge distribution in the solid state. Characteristic features in the electronic spectra of each valence tautomer have

Table 4. Atomic Coordinates ($\times 10^4$) and Equivalent Isotropic Displacement Parameters (Å^2, $\times 10^3$) for Selected Atoms of Mn^{II}(NO$_2$-phen)(3,6-DBSQ)$_2$

	x/a	*y/b*	*z/c*	*U*(eq)
Mn	0	726(1)	0	47(1)
O1	1256(5)	1431(5)	937(3)	53(3)
O2	1241(6)	−599(6)	251(4)	56(3)
C1	2107(8)	829(9)	1157(5)	46(4)
C2	2085(8)	−334(9)	781(6)	52(4)
C3	2983(9)	−1134(9)	993(6)	59(5)
C4	3872(9)	−731(11)	1546(6)	71(5)
C5	3903(8)	403(10)	1895(6)	70(5)
C6	3042(9)	1202(10)	1727(6)	51(4)
O3	−1256(5)	1382(5)	479(3)	56(3)
O4	−1167(5)	−668(6)	−155(4)	65(3)
C15	−2117(8)	755(9)	370(5)	50(4)
C16	−2043(8)	−421(9)	36(5)	53(4)
C17	−2904(9)	−1265(9)	−68(6)	53(4)
C18	−3791(9)	−868(10)	127(6)	72(5)
C19	−3886(8)	296(10)	416(7)	77(5)
C20	−3083(8)	1129(9)	556(6)	49(4)
N1	−11(6)	2579(6)	−512(5)	46(3)
N2	−5(5)	553(11)	−1275(5)	60(4)
C29	−1(7)	2675(11)	−1265(6)	47(4)
C30	9(8)	3798(13)	−1601(7)	64(5)
C31	15(9)	4777(12)	−1336(9)	79(6)
C32	23(9)	4657(11)	−386(8)	77(6)
C33	24(11)	3525(9)	−87(8)	62(4)
C34	2(7)	1582(12)	−1680(8)	61(5)
C35	25(8)	1651(16)	−2459(8)	77(7)
C36	25(11)	529(22)	−2814(11)	116(10)
C37	−5(11)	−509(18)	−2401(13)	105(9)
C38	−39(9)	−423(12)	−1665(9)	79(6)
C39	53(10)	3779(16)	−2402(11)	83(8)
C40	43(11)	2810(22)	−2783(8)	98(8)
N3	35(12)	4846(17)	−2861(11)	127(8)
O5	262(14)	4876(13)	−3442(8)	200(10)
O6	−176(14)	5757(13)	−2626(9)	188(10)

Table 5. Atomic Coordinates ($\times 10^4$) and Equivalent Isotropic Displacement Parameters (Å^2, $\times 10^3$) for Selected Atoms of Mn(phen)(3,6-DBQ)$_2$

	x/a	*y/b*	*z/c*	*U*(eq)
Mn	0	880(1)	2500	51(1)
O1	1867(2)	893(1)	3613(2)	57(1)
O2	−261(2)	1285(1)	3552(3)	67(1)
C1	2143(3)	1218(1)	4379(3)	45(2)
C2	949(3)	1444(1)	4335(3)	47(2)
C3	1058(4)	1803(1)	5041(3)	50(2)
C4	2393(4)	1912(1)	5816(3)	61(2)
C5	3566(4)	1686(1)	5869(3)	59(2)
C6	3494(3)	1338(1)	5158(3)	45(2)
N1	702(3)	347(1)	1823(3)	55(1)
C15	400(4)	−41(1)	2150(3)	55(2)
C16	835(5)	−425(1)	1839(4)	77(2)
C17	1655(6)	−396(2)	1190(5)	99(3)
C18	1978(5)	−5(2)	893(5)	98(3)
C19	1478(4)	364(2)	1212(4)	76(2)
C20	401(5)	−814(1)	2199(5)	106(3)

(8) See for example: Vlcek, A., Jr. *J. Organomet. Chem.* **1986**, *306*, 63.

(9) Attia, A. S.; Pierpont, C. G. Manuscript in preparation.

Table 6. Selected Bond Lengths (Å) for $Mn(2,2'\text{-bpy})(3,6\text{-DBCat})_2$, $Mn(4,4'\text{-bpy})_2(3,6\text{-DBSQ})(3,6\text{-DBCat})\cdot 2C_4H_8O_2$, $Mn(NO_2\text{-phen})(3,6\text{-DBSQ})_2\cdot 2C_7H_8$, and $Mn(phen)(3,6\text{-DBQ})_2$

	$Mn^{IV}(2,2'\text{-bpy})(3,6\text{-DBCat})_2$	$Mn(phen)(3,6\text{-DBQ})_2$	$Mn^{III}(4,4'\text{-bpy})_2(3,6\text{-DBSQ})(3,6\text{-DBCat})$	$Mn^{II}(NO_2\text{-phen})(3,6\text{-DBSQ})_2$[a]
Mn−O1	1.866(2)	1.881(2)	1.889(5)	2.139(5)
Mn−O2	1.867(2)	1.906(3)	1.883(4)	
Mn−N	2.086(2)	2.120(4)	2.273(7)	2.290(6)
O1−C1	1.354(4)	1.333(4)	1.334(7)	1.271(8)
O2−C2	1.355(3)	1.339(4)	1.336(8)	
C1−C2	1.408(4)	1.421(5)	1.403(10)	1.471(8)
C2−C3	1.390(5)	1.392(5)	1.421(8)	1.424(8)
C3−C4	1.395(4)	1.380(5)	1.377(11)	1.369(9)
C4−C5	1.389(5)	1.396(6)	1.390(11)	1.426(9)
C5−C6	1.383(5)	1.378(5)	1.389(9)	
C1−C6	1.396(4)	1.402(4)	1.416(10)	

[a] Averaged values for two independent ligands.

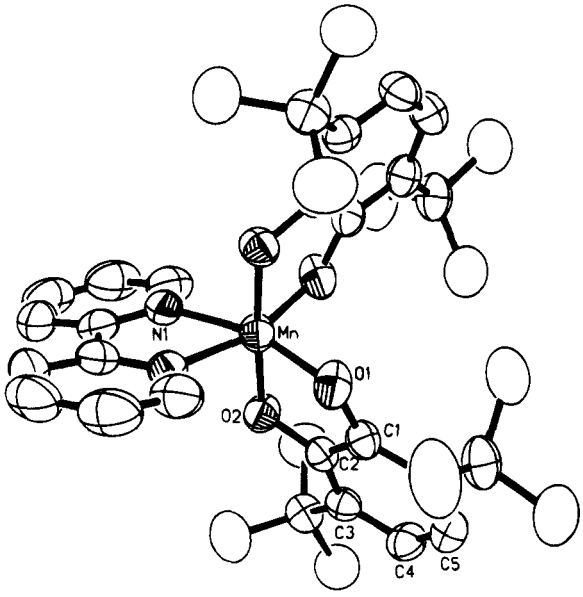

Figure 1. View of $Mn^{IV}(2,2'\text{-bpy})(3,6\text{-DBCat})_2$.

been used to monitor temperature-dependent shifts in tautomeric equilibria for samples in solution and in the solid state.

$Mn^{IV}(2,2'\text{-bpy})(3,6\text{-DBCat})_2$. Photolysis of a solution containing $Mn_2(CO)_{10}$, 3,6-DBBQ, and 2,2'-bpy gives $Mn^{IV}(2,2'\text{-bpy})(3,6\text{-DBCat})_2$. A view of the molecule is shown in Figure 1, and selected bond lengths and angles are given in Table 6. Short Mn−O and Mn−N bond lengths point characteristically to the d^3 $Mn^{IV}(Cat)_2$ charge distribution. The average Mn−O length of 1.867(2) Å and the Mn−N length of 2.086(2) Å agree well with the Mn−O and Mn−N lengths of 1.854(2) and 2.018(3) Å for *trans*-$Mn(py)_2(3,5\text{-DBCat})_2$, and they are in accord with the lengths observed for other Mn(IV) complexes containing nitrogen- and oxygen-donor ligands.[10] Moreover, they fail show the Jahn−Teller distortion that appears characteristically for high-spin d^4 Mn(III).[11] The crystal structure consists of polymeric stacks of complex molecules, linked by overlapped pyridine rings of adjacent bipyridine ligands (Figure 2). Similar intermolecular stacking contributes to the cooperative photomechanical properties of isostructural $Co(bpy)(3,6\text{-DBSQ})(3,6\text{-DBCat})$.[2b,3a] Magnetic measurements carried out at room temperature and 100 K gave moments of 3.91 and 3.87 μ_B (Table 7), values that are typical of $S = {}^3/_2$ Mn(IV). Optical spectra recorded on a solid sample of $Mn(2,2'\text{-bpy})(3,6\text{-DBCat})_2$ show two intense transitions at 440 and 750 nm that are responsible for the intense purple color of the complex and compare with related transitions at 515 and 824 nm for purple $Mn^{IV}(py)_2(3,5\text{-DBCat})_2$ in toluene solution at 232 K. No absorptions appear for the complex at lower energy.

$Mn^{III}(4,4'\text{-bpy})_2(3,6\text{-DBSQ})(3,6\text{-DBCat})$. Purple crystals of $Mn^{III}(4,4'\text{-bpy})_2(3,6\text{-DBSQ})(3,6\text{-DBCat})$ have been characterized crystallographically. A view of the complex molecule is shown in Figure 3, and bond lengths and angles are listed in Table 6. The molecule is located about a crystallographic inversion center that requires a *trans* coordination geometry and superimposes the quinone ligands. The average Mn−O length of 1.886(4) Å is slightly longer than the values for *trans*-$Mn^{IV}(py)_2(3,5\text{-DBCat})_2$ and $Mn^{IV}(bpy)(3,6\text{-DBCat})_2$, but it agrees with the Mn^{III}−O length of 1.910(1) Å for the axially-distorted $[Mn^{III}(acac)_2(N_3)]_n$ polymer.[11a] The axial Mn−N length of 2.273(7) Å is characteristic of high-spin Mn(III). Features of the coordination polyhedron point uniquely to the *trans*-$Mn^{III}(4,4'\text{-bpy})_2(3,6\text{-DBSQ})(3,6\text{-DBCat})$ charge distribution with quinone ligands of mixed charge. Bond lengths within the unique quinone ligand reflect an average of Cat and SQ values with intermediate C−O lengths and values for the C3−C4 and C5−C6 bonds that are slightly shorter than those for other C−C bonds of the ring. Either the dissimilar ligands are charge localized and disordered or they are delocalized. Infrared spectra in the region between 1000 and 1400 cm^{-1}, the region most sensitive to quinone ligand charge,[12] show two broad bands that fail to clearly resolve the question.

The difference in charge distribution between $Mn^{IV}(2,2'\text{-bpy})(3,6\text{-DBCat})_2$ and $Mn^{III}(4,4'\text{-bpy})_2(3,6\text{-DBSQ})(3,6\text{-DBCat})$ may give rise to a difference in magnetic properties. However, the spin of the radical SQ ligand is in a π-orbital that interacts antiferromagnetically with a metal $d\pi$ spin. This is the case; magnetic moment drops from a value of 4.26 μ_B at 350 K to 3.69 μ_B at 10.6 K as shown in Figure 4, and there is little difference between the magnetic properties of $Mn^{IV}(2,2'\text{-bpy})(3,6\text{-DBCat})_2$ and $Mn^{III}(4,4'\text{-bpy})_2(3,6\text{-DBSQ})(3,6\text{-DBCat})$. Optical spectra have been measured for $Mn^{III}(4,4'\text{-bpy})_2(3,6\text{-DBSQ})(3,6\text{-DBCat})$ in the solid state to note unique features that may appear characteristically for the $Mn^{III}(SQ)(Cat)$ tautomers. Surprisingly, the UV−vis region appears similar to the spectra of $Mn(2,2'\text{-bpy})(3,6\text{-DBCat})_2$ and $Mn(py)_2(3,5\text{-DBCat})_2$ with intense transitions at 550 and 880 nm that give the intense purple color of all three complexes of both charge distributions. This is clearly why the $Mn^{III}(py)_2(3,5\text{-DBSQ})(3,5\text{-DBCat})$ species was unobserved in the investigation carried out earlier.

(10) (a) Camenzind, M. J.; Hollander, F. J.; Hill, C. L. *Inorg. Chem.* **1982**, *21*, 4301. (b) Gohdes, J. W.; Armstrong, W. H. *Inorg. Chem.* **1992**, *31*, 368. (c) Larson, E.; Lah, M. S.; Li, X.; Bonadies, J. A.; Pecoraro, V. L. *Inorg. Chem.* **1992**, *31*, 373.

(11) (a) Stults, B. R.; Marianelli, R. S.; Day, V. W. *Inorg. Chem.* **1975**, *14*, 722. (b) Sarneski, J. E.; Brzezinski, L. J.; Anderson, B.; Didiuk, M.; Manchanda, R.; Crabtree, R. H.; Brudvig, G. W.; Schulte, G. K. *Inorg. Chem.* **1993**, *32*, 3265. (c) Bouwman, E.; Caulton, K. G.; Christou, G.; Folting, K.; Gasser, C.; Hendrickson, D. N.; Huffman, J. C.; Lobkovsky, E. B.; Martin, J. D.; Michel, P.; Tsai, H.-L.; Xue, Z. *Inorg. Chem.* **1993**, *32*, 3463.

(12) Haga, M.; Isobe, K.; Boone, S. R.; Pierpont, C. G. *Inorg. Chem.* **1990**, *29*, 3795.

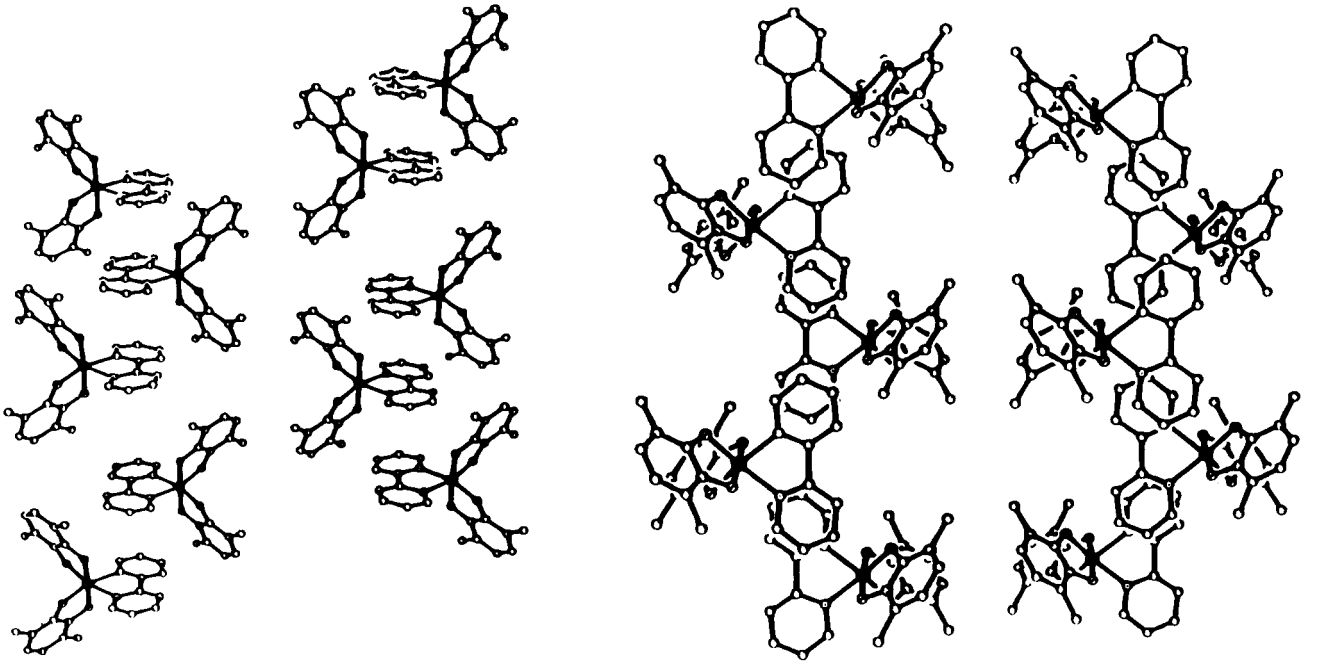

Figure 2. Intermolecular stacking in the crystal structure of Mn(2,2′-bpy)(3,6-DBCat)$_2$.

Table 7. Magnetic and Spectroscopic Data for Members of the Mn(N-N)(3,6-DBQ)$_2$ Series

	magnetic moment (μ_B)		optical transitions (nm)[b]	
	10 K	350 K	vis	IR
Mn^{IV}(2,2′-bpy)(3,6-DBCat)$_2$		3.91[a]	440, 750	2070
Mn^{IV}(py)$_2$(3,6-DBCat)$_2$		3.88[a]	545, 853	2130
Mn(phen)(3,6-DBQ)$_2$	3.69	3.99	438, 752	2030
Mn^{III}(4,4′-bpy)$_2$(3,6-DBSQ)(3,6-DBCat)	3.68	4.26	555, 880	2170
Mn^{II}(NO$_2$-phen)(3,6-DBSQ)$_2$	3.71	4.36	448, 728	

[a] Values measured at 296 K. [b] Samples prepared as KBr pellets.

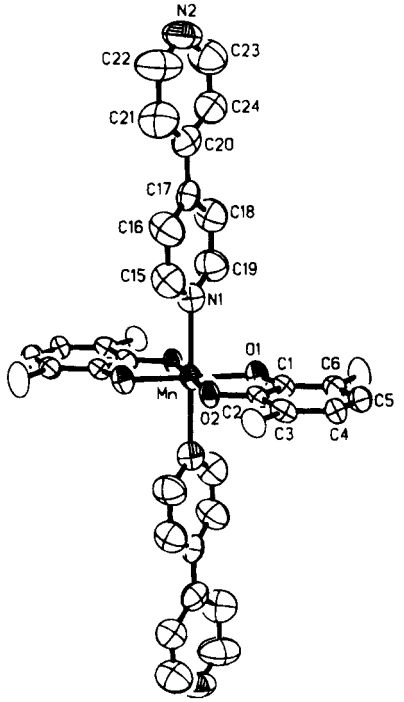

Figure 3. View of Mn^{III}(4,4′-bpy)$_2$(3,6-DBSQ)(3,6-DBCat).

A unique feature that is characteristic of the Mn^{III}(SQ)(Cat) tautomer appears at lower energy as an intense transition centered near 2170 nm (Figure 5). Similar bands have been observed for *trans*-Mn^{III}(py)$_2$(3,6-DBSQ)(3,6-DBCat) (2130 nm), the [*trans*-Mn^{III}(pyz)(3,6-DBSQ)(3,6-DBCat)]$_n$ polymer (2080 nm), *trans*-Mn^{III}(thf)$_2$(3,6-DBSQ)(3,6-DBCat) (2100 nm), and Mn^{III}(3,6-DBSQ)$_3$ (2300 nm).[9]

Mn^{II}(NO$_2$-phen)(3,6-DBSQ)$_2$. As with Mn^{IV}(bpy)(3,6-DBCat)$_2$ and Mn^{III}(4,4′-bpy)$_2$(3,6-DBSQ)(3,6-DBCat), the structural features of Mn^{II}(NO$_2$-phen)(3,6-DBSQ)$_2$ point to a specific oxidation state for the metal. The coordination geometry, shown in Figure 6 with bond lengths and angles listed in Table 6, is trigonal prismatic with a twist angle between triangular faces of the prism that is less than 4°. Average Mn−O and Mn−N lengths of 2.139(5) and 2.290(6) Å are typical values for high-spin Mn(II), and the prismatic structure generally occurs for metal ions that lack stereochemical preference.[13] In this case also, a change in magnetic moment may accompany the shift in charge distribution. However, the radical spins of the two SQ ligands couple with two metal dπ spins to give a moment that is close to that expected for a $S = {}^3/_2$ ground state. The magnetic moment of Mn^{II}(NO$_2$-phen)(3,6-DBSQ)$_2$ decreases from 4.36 μ_B at 350 K to 3.50 μ_B at 5 K (Table 7, Figure 4). Optical spectra recorded on a solid sample prepared as a KBr pellet are similar to spectra observed for the [Mn^{II}(3,5-DBSQ)$_2$]$_4$ tetramer and for toluene solutions of Mn^{II}(py)$_2$(3,5-DBSQ)$_2$ at room temperature.[6] Low-intensity spectral bands appear for all three complexes of the Mn^{II}(SQ)$_2$ charge distribution in the 420 and 750 nm regions, with no other transitions to lower energy.

Valence Tautomeric Equilibria: Mn(phen)(3,6-DBQ)$_2$. The results of studies on coligand bonding effects for the Co(N-N)(SQ)(Cat) series indicated that the 9,10-phenanthroline (phen) ligand may be useful in forming a manganese complex consisting of a mixture of tautomers in the solid state at room

(13) Diril, H.; Chang, H.-R.; Zhang, X.; Larsen, S. K.; Potenza, J. A.; Pierpont, C. G.; Schugar, H. J.; Isied, S. S.; Hendrickson, D. N. *J. Am. Chem. Soc.* **1987**, *109*, 6207.

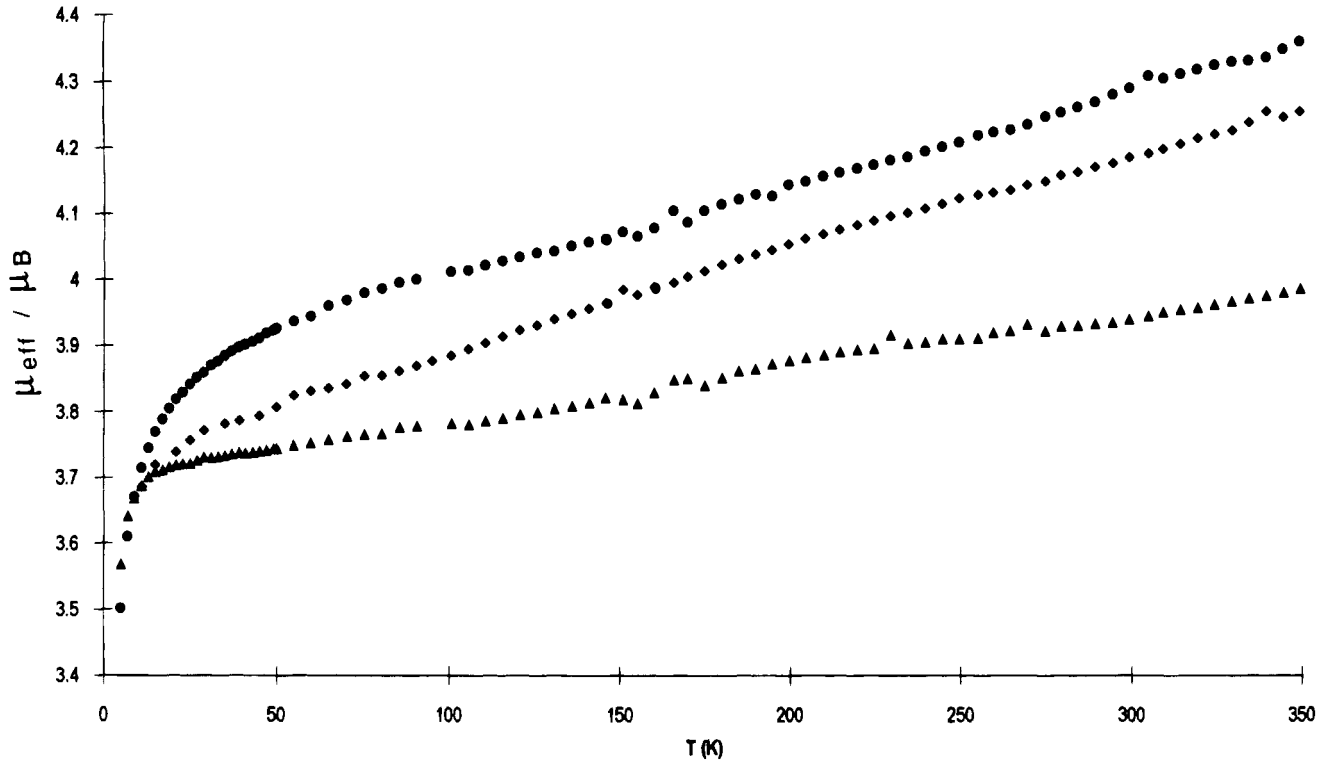

Figure 4. Temperature-dependent magnetic properties of $Mn^{III}(4,4'\text{-bpy})_2(3,6\text{-DBSQ})(3,6\text{-DBCat})$ (◆), $Mn^{II}(NO_2\text{-phen})(3,6\text{-DBSQ})_2$ (●), and $Mn(phen)(3,6\text{-DBQ})_2$ (▲).

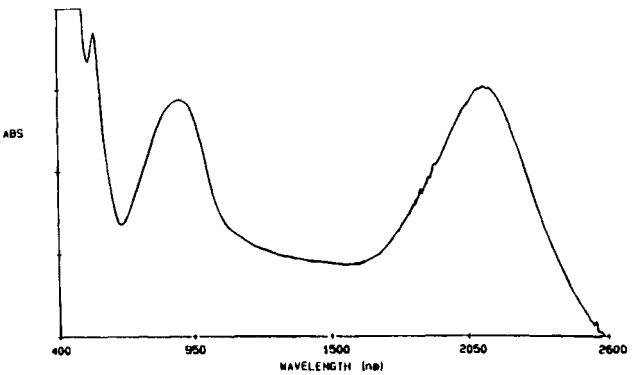

Figure 5. Solid state electronic spectrum of $Mn^{III}(4,4'\text{-bpy})_2(3,6\text{-DBSQ})(3,6\text{-DBCat})$ (KBr).

temperature.[2,3] The crystal structure of $Mn(phen)(3,6\text{-DBQ})_2$ is similar to that of $Mn^{IV}(2,2'\text{-bpy})(3,6\text{-DBCat})_2$ with one-dimensional stacks of complex units paired by overlapped regions of adjacent phen ligands. The complex molecule, shown in Figure 7 with bond lengths and angles listed in Table 6, is grossly similar to the 2,2′-bpy analog, but with subtle differences in bond lengths. The average Mn−O and Mn−N lengths of $Mn(phen)(3,6\text{-DBQ})_2$ are both 0.03 Å longer than lengths of $Mn(2,2'\text{-bpy})(3,6\text{-DBCat})_2$ and the two Mn−O lengths differ by 10σ. Lengths of bonds to the metal are not those of a tetragonally distorted d^4 Mn(III) complex but appear intermediate between those for Mn(IV) and Mn(III) complexes. Features of the optical spectrum are more sensitive to charge distribution in the sample. $Mn(phen)(3,6\text{-DBQ})_2$ is purple and similar to the $Mn^{IV}(Cat)_2$ and $Mn^{III}(SQ)(Cat)$ tautomers in showing intense transitions at 438 and 752 nm. In addition, a band of moderate intensity appears for the complex at 2030 nm that is characteristic of $Mn^{III}(phen)(3,6\text{-DBSQ})(3,6\text{-DBCat})$. The intensity of this band increases reversibly with increasing sample temperature to 350 K and decreases with a decrease in temperature. These observations are similar to the spectral

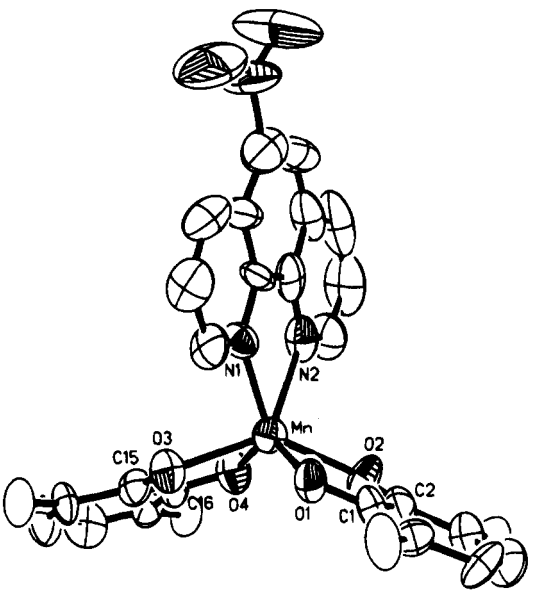

Figure 6. View of $Mn^{II}(NO_2\text{-phen})(3,6\text{-DBSQ})_2$.

changes in the 2500 nm region associated with the $Co^{III}(N\text{-}N)(SQ)(Cat)/Co^{II}(N\text{-}N)(SQ)_2$ tautomeric equilibrium[2b] and correspond to shifts in the $Mn^{IV}(Cat)_2/Mn^{III}(SQ)(Cat)$ equilibrium shown in eq 3. As in the case of the cobalt series, the oxidized-

$$Mn^{IV}(phen)(DBCat)_2 \rightleftharpoons Mn^{III}(phen)(DBSQ)(DBCat) \quad (3)$$

metal reduced-quinone tautomer, $Mn^{IV}(Cat)_2$, is favored at low temperature.

With this information, we returned to the spectrum of $Mn^{IV}(2,2'\text{-bpy})(3,6\text{-DBCat})_2$. Structural features of the complex indicate that it is exclusively in the Mn(IV) charge distribution at room temperature in the solid state, and the absence of band intensity in the 2100 mn region confirms this. Upon heating

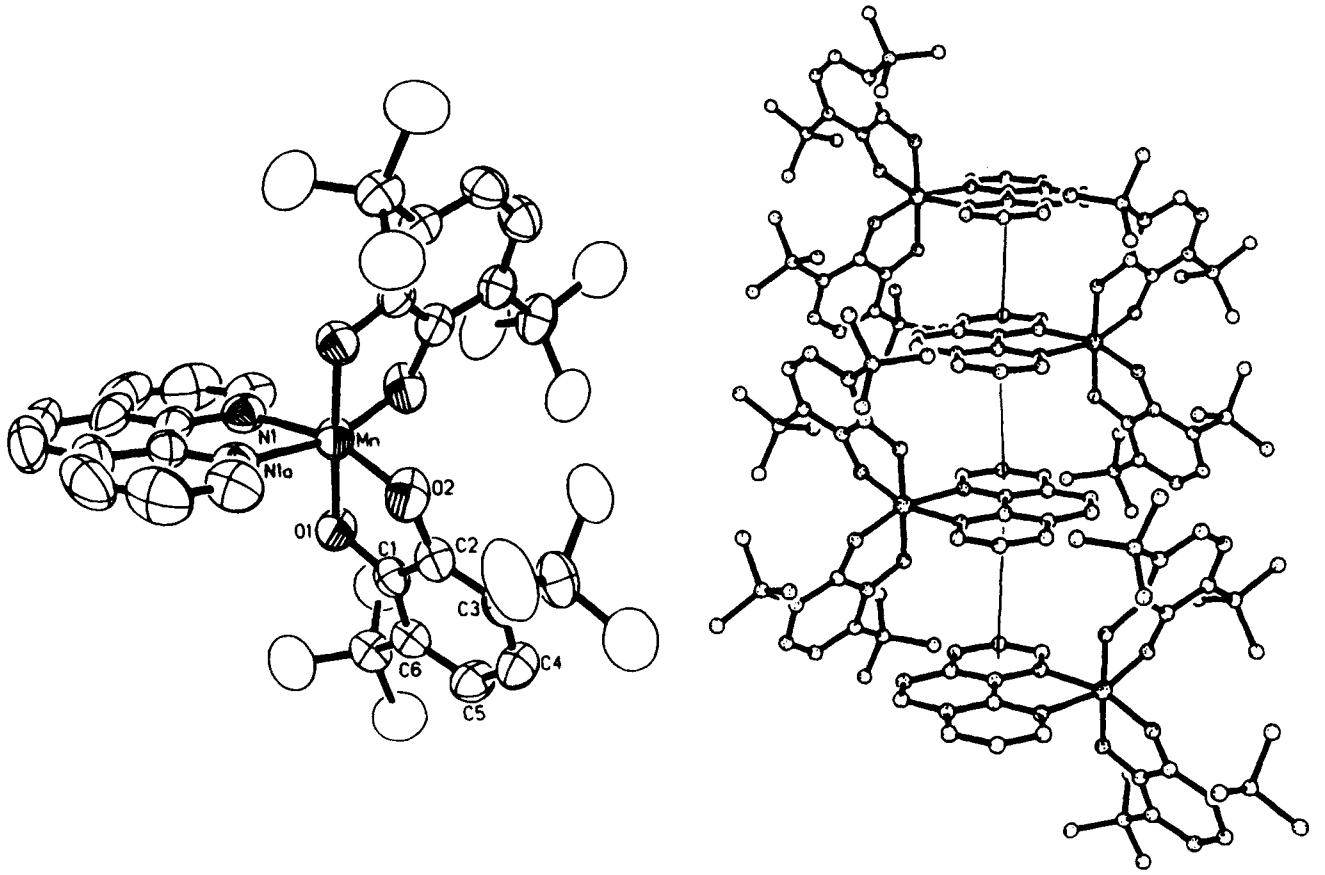

Figure 7. View of Mn(phen)(3,6-DBQ)$_2$ with intermolecular stacking between phen ligands.

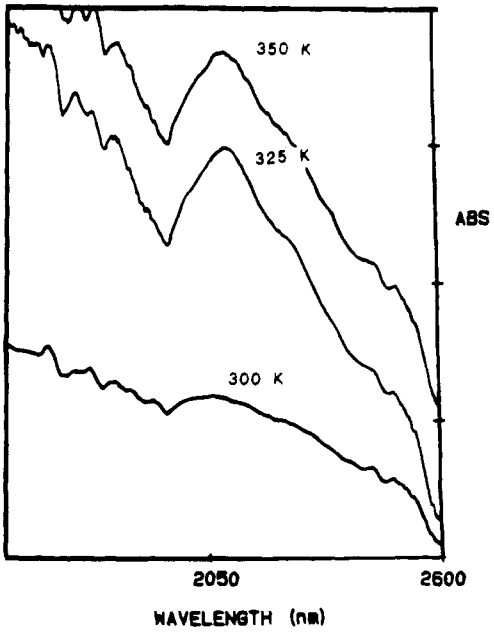

Figure 8. Appearance of the 2070 nm transition of Mn^{III}(2,2′-bpy)(3,6-DBSQ)(3,6-DBCat) at increased temperature in the solid state (KBr).

of the sample to 350 K, increases in absorbance at 2070 nm, shown in Figure 8, indicate a shift to Mn^{III}(2,2′-bpy)(3,6-DBSQ)(3,6-DBCat), and upon cooling of the sample to room temperature, band intensity decreases reversibly. Similar experiments carried out with Mn^{III}(4,4′-bpy)$_2$(3,6-DBSQ)(3,6-DBCat) led to a different result. In this case, band intensity at 2170 nm decreased with increasing temperature with a corresponding decrease in intensity at 880 and 550 nm. The shift in equilibrium responsible for this spectral change involves the Mn^{II}(4,4′-bpy)$_2$(3,6-DBSQ)$_2$ tautomer (eq 4). In toluene solution

$$\text{Mn}^{III}(4,4'\text{-bpy})_2(\text{DBSQ})(\text{DBCat}) \rightleftharpoons \text{Mn}^{II}(4,4'\text{-bpy})_2(\text{DBSQ})_2 \quad (4)$$

at temperatures near room temperature, all complexes of the series shift to the Mn^{II}(N-N)(3,6-DBSQ)$_2$ charge distribution. The Mn(II) tautomers are subject to ligand dissociation in solution at room temperature. Temperature-dependent spectral changes of the type reported earlier for *trans*-Mn(py)$_2$(3,5-DBQ)$_2$ may be observed with a dramatic change in the color of the solution, from the pale green-brown of the Mn(II) tautomer to the intense purple of the Mn(III)/Mn(IV) mixture.[6] Quantitative studies on solution equilibrium concentrations have been complicated by band overlap in the UV−vis and spectral noise in the 2000 nm region associated with vibrational activity of the solvent, cuvette, and cryostat windows. These difficulties are being resolved, and it should be possible to obtain thermodynamic values for both steps in the tautomeric equilibria. However, with the temperature separation between steps, it may be impossible to observe both steps for a single complex under similar experimental conditions.

Discussion

The unique electron transfer properties of the Co(N-N)(DBQ)$_2$ series raise questions about the generality of this property for quinone complexes of other redox-active metal ions. With the complexes included in this series, we have been able to provide structural and spectral characterization of representative examples in all three tautomeric charge distributions of the Mn(N-N)(3,6-DBQ)$_2$ series. The two-electron equilibrium described in eq 2 occurs in two one-electron steps:

$$\underset{(d\pi)^3(d\sigma)^0(\pi_{Q1})^2(\pi_{Q2})^2}{Mn^{IV}(N\text{-}N)(Cat)_2} \rightleftarrows \underset{(d\pi)^3(d\sigma)^1(\pi_{Q1})^2(\pi_{Q2})^1}{Mn^{III}(N\text{-}N)(SQ)(Cat)}$$

$$\underset{(d\pi)^3(d\sigma)^1(\pi_{Q1})^2(\pi_{Q2})^1}{Mn^{III}(N\text{-}N)(SQ)(Cat)} \rightleftarrows \underset{(d\pi)^3(d\sigma)^2(\pi_{Q1})^1(\pi_{Q2})^1}{Mn^{II}(N\text{-}N)(SQ)_2}$$

Coligand bonding properties define the Mn(IV)/Mn(III) and Mn(III)/Mn(II) transition temperatures, the Mn(IV) isomer is favored at low temperature and in polar solvent media, and the pattern of coligand dependence follows observations made on the Co series.[2] For the $MnL_2(3,6\text{-}DBQ)_2$ series in the solid state at room temperature, 2,2′-bpy gives a product that is almost entirely in the Mn(IV) form. Pyridine ligands in *trans*-Mn(py)$_2$(3,6-DBQ)$_2$ give a product that is predominantly the Mn(IV) isomer at room temperature, but the appearance of a weak transition at 2130 nm indicates the low-level presence of the Mn(III) tautomer. The properties of Mn(phen)(3,6-DBQ)$_2$ indicate that it also is a mix of Mn(IV) and Mn(III) isomers, but structure and band intensity at 2030 nm indicate that the Mn(III) tautomer is favored at room temperature. Complexes containing the 4,4′-bpy, thf, and pyz coligands all have been found to have *trans* structures, features indicative of the Mn(III) charge distribution, and intense transitions in the 2100 nm region. Upon heating of samples of these complexes, band intensity decreases in a way that is consistent with an equilibrium shift from the Mn(III) tautomer toward Mn(II) in eq 4. Finally, with NO_2-phen, the product is exclusively in the Mn(II) tautomeric form. The pattern of coligand influence for the complexes of both Co and Mn fails to follow the order of π-acceptor strength.[14] In fact, in the Co series, 2,2′-bpy and tmeda are similar, and with Mn, 4,4′-bpy and thf are similar. It may be concluded that coligand donation is most important in determining charge distribution through enthalpic contributions that are similar to those that define the transition temperatures of related complexes of cobalt.[2b] The relative properties of *cis* complexes containing chelating coligands and *trans* complexes containing independent pyridine-derived ligands indicate that the shift in stereochemistry about the metal has little influence on charge distribution.[15]

Tautomeric equilibria have been observed to occur in the solid state, a property that is of considerable importance for practical applications. Magnetic measurements fail to provide information on the relative concentrations of tautomers due to competing effects of Mn−SQ magnetic exchange. However, the intensity of the 2100 nm transition that appears characteristically for the Mn(III) tautomer may be used to monitor shifts in both tautomeric equilibria. A pattern is beginning to develop between the appearance of intense low-energy electronic transitions and complexes that show valence tautomerc equilibria. Other examples include the oligomeric stacks of $Rh^I(CO)_2$(3,6-DBSQ) units that show a charge transfer transition in the 1600 nm region[5] and the Co^{III}(N-N)(SQ)(Cat) tautomers that have transitions in the 2500 nm region.[2a] Members of both series show cooperative thermal and photophysical properties in the solid state that are associated with changes in molecular volume coupled with low-energy metal−quinone electron transfer. Similar effects may be observed for members of the manganese series, although, the 2100 nm optical transition fails to show the coligand-dependent pattern that would be expected for a charge transfer transition involving a metal electronic level. In general, transitions of the *trans* complexes (Table 7) appear at slightly lower energies than those of the 2,2′-bpy and phen complexes, but there is no correlation with coligand donation or charge distribution at room temperature. A relatively strong coligand dependence was observed for members of the Co(N-N)(3,6-DBQ)$_2$ series that led to an assignment for the 2500 nm transition as a Cat → Co(III) transition. For the manganese series, an alternative assignment as a metal-mediated Cat → SQ interligand charge transfer band is possible for the 2100 nm transition.[9] However, members of the iron series, Fe^{III}(N-N)(SQ)(Cat), fail to show transitions at low energy and fail to exhibit tautomeric equilibria, reinforcing the idea that these transitions are associated with low-energy Cat → M(III) electron transfer.

Manganese−quinone electron transfer results from the close energy separation between metal and quinone electronic levels. Ligand field effects are primarily responsible for creating the balance in orbital energies, and donation contributes enthalpically to coligand-dependent differences in charge distribution.[2b] The thermal dependence of equilibria is entropic, and consideration of the contributions to the intramolecular entropy change (ΔS_{intra}) associated with redox couples provides a model for estimating the relative importance of contributions from electronic and vibrational effects.[16] As a general paradigm, the addition of charge to M−L σ-antibonding orbitals results in a large positive entropy change through the increase in low-frequency vibrational activity. Quantitatively, for the low-spin Co(III)/high-spin Co(II) couple, this is the most significant contribution to ΔS_{intra} as reduction results in an increase in Co−L bond length of roughly 0.2 Å. Positive contributions to ΔS_{intra} from changes in orbital and spin degeneracy are less significant. The total entropy change should include consideration of contributions from solvation, but for complexes containing the 3,5-DBQ and 3,6-DBQ ligands, these effects are found to be small.[17] This model has been used in the analysis of Co^{III}(bpy)(3,5-DBSQ)(3,5-DBCat)/Co^{II}(bpy)(3,5-DBSQ)$_2$ equilibria in solution and in the solid state.[17] Changes in bond length and complex spin state are similar for the manganese series, and the contributions to ΔS_{intra} that are responsible for the Co(III)/Co(II) tautomeric equilibria also apply to the transition from Mn^{IV}(N-N)(Cat)$_2$ to Mn^{II}(N-N)(SQ)$_2$. Further, the observation of trigonal prismatic forms of the Co(II) and Mn(II) complexes points to an additional entropic contribution from the increase in conformational flexibility of the reduced metal ions in solution. Metal−quinone electron transfer may occur at low energy for many metal ions,[18] but the positive entropic effects that are responsible for the temperature-dependent valence tautomeric equilibria are, so far, restricted to the complexes of Co and Mn.

Acknowledgment. We thank Brenda Conklin for recording magnetic susceptibility measurements and Professor M. F. El-Shahat of Ain Shams University for helpful comments. Support for this research was provided by the National Science Foundation through Grant CHE 90-23636 and the Egyptian Ministry of Science (A.S.A.) through a Graduate Fellowship.

Supplementary Material Available: Tables giving crystal data and details of the structure determinations, atomic coordinates, anisotropic thermal parameters, hydrogen atom locations, and bond lengths and angles for Mn(2,2′-bpy)(3,6-DBCat)$_2$, Mn(4,4′-bpy)$_2$(3,6-DBSQ)(3,6-DBCat), Mn(phen)(3,6-DBSQ)(3,6-DBCat), and Mn(NO_2-phen)(3,6-DBSQ)$_2$ (44 pages). Ordering information is given on any current masthead page.

IC941371H

(14) (a) Kriley, C. E.; Fanwick, P. E.; Rothwell, I. P. *J. Am. Chem. Soc.* **1994**, *116*, 5225. (b) Cloninger, K. K.; Callahan, R. W. *Inorg. Chem.* **1981**, *20*, 1611.
(15) Attia, A. S.; Jung, O.-S.; Pierpont, C. G. *Inorg. Chim. Acta* **1994**, *226*, 91.
(16) Richardson, D. E.; Sharpe, P. *Inorg. Chem.* **1991**, *30*, 1412.
(17) Pierpont, C. G.; Jung, O.-S. *Inorg. Chem.*, in press.
(18) Dei, A. *Inorg. Chem.* **1993**, *32*, 5730.